# Study of the $\bar{p}p \to \bar{n}n$ reaction in the momentum range 480 to 728 MeV/$c$

T. Tsuboyama, Y. Kubota,* F. Sai, S. Sakamoto, and S. S. Yamamoto
*Department of Physics, University of Tokyo, Bunkyo-ku, Tokyo 113, Japan*
(Received 27 April 1983; revised manuscript received 5 July 1983)

The total and differential $\bar{p}p$ charge-exchange cross sections were obtained at seven momenta in the range 480 to 728 MeV/$c$. The total cross sections are roughly consistent with other data. The momentum dependences of the Legendre coefficients $a_1/a_0$, $a_2/a_0$, and $a_3/a_0$ of the differential cross sections do not agree well with the predictions of the Bryan-Phillips model, unlike the case of elastic scattering.

## I. INTRODUCTION

One of the least-studied $\bar{p}p$ reactions is the charge-exchange reaction despite its importance to the understanding of the antinucleon-nucleon interaction. Unlike its charge-symmetric reaction, the elastic-scattering reaction, the charge-exchange reaction is difficult to detect and analyze, since the final state is all neutral. Therefore, only a handful of experiments have been done on this reaction in the incident-momentum range below 1 GeV/$c$. There are only two high-statistics measurements of the total cross section over this momentum range,[1,2] one high-statistics measurement of the differential cross section in the range 700–760 MeV/$c$,[3] and one at 696 MeV/$c$.[4] Differential cross sections have also been measured at 11 momenta in the range 350–800 MeV/$c$,[5] at 2 momenta in the range 310–608 MeV/$c$,[6] and at 9 momenta in the range 275–534 MeV/$c$.[7]

In this paper we present the result of an analysis of the $\bar{p}p$ charge-exchange reaction at seven incident momenta of 480, 537, 584, 630, 670, 698, and 728 MeV/$c$, using the Brookhaven-Columbia 30-in. bubble chamber. The analysis is based on 1385 events, which is comparable to or better than the previous experiments[5–7] in statistics. The details of the experimental arrangement have already been reported.[8]

## II. EVENT SELECTION

The 245 000 pictures used for this analysis were double scanned for the zero-prong plus three-, five-, or seven-prong star topologies. The scanning efficiency was a little over 90% for all momenta and topologies.

The events found in scanning were measured and spatially reconstructed in a standard way. Up to two remeasurements were made for events failing spatial reconstruction. Less than 1% of the scanned events failed spatial reconstruction after two remeasurements, and were neglected in the analysis.

The spatially reconstructed events were fitted to the following kinematical hypotheses (the $\bar{n}p$ annihilation cross section into states containing $K\bar{K}$ amounts to less than 1% of the total annihilation cross section,[9] and was neglected in the following analysis):

$\bar{p}p \to \bar{n}n$ followed by $\bar{n}p \to 2\pi^+\pi^-$

$2\pi^+\pi^-\pi^0$

$3\pi^+2\pi^-$

$3\pi^+2\pi^-\pi^0$

$4\pi^+3\pi^-$

$4\pi^+3\pi^-\pi^0$ .

Since more than one $\pi^0$ is often involved in antinucleon-nucleon annihilation, not all events actually fitted the above hypotheses. Therefore, all spatially reconstructed events were looked at on the scanning table to make sure that the ionization of the tracks was consistent with their being pions.

The reactions which have the same topology as the three-prong $\bar{n}p$ annihilation star are off-beam $pp \to pp$, $\bar{p}p \to \bar{p}p$, $\pi^\pm p \to \pi^\pm p$, and $\pi^+p \to \pi^\pm\pi^+n$ reactions. If any of these reactions is accidentally present downstream of a zero-prong event, it will have the zero-prong plus three-prong star topology. The first three reactions are easy to identify on the basis of track ionization, since they include at least one proton in the final state. The last reaction can be identified if one of the tracks is seen going toward the annihilation vertex by means of a $\delta$ ray.

In order to ascertain that events were properly selected, we looked at the coplanarity of the accepted three-prong stars. Coplanarity is defined as the cosine of the angle between the normal to the plane formed by any two tracks and the direction of the remaining track. Figure 1(a) shows the coplanarity distribution of the accepted events. The curve is the result of a Monte Carlo simulation based on the $\bar{n}$ momentum distribution of the fitted events and the fractions of the pionic annihilation reactions obtained from $\bar{p}n$ reactions.[10] The coplanarity distribution shows no anomalous behavior.

To check that the $\pi^\pm p \to \pi^\pm\pi^+n$ reaction was not contaminating our sample, a missing-mass distribution against $\pi^\pm\pi^+$ was obtained, using the track with the highest momentum as the incident track. The distribution is shown in Fig. 1(b). The curve is the result of the same Monte Carlo simulation described above. Again no anomalous behavior is observed in the distribution.

 

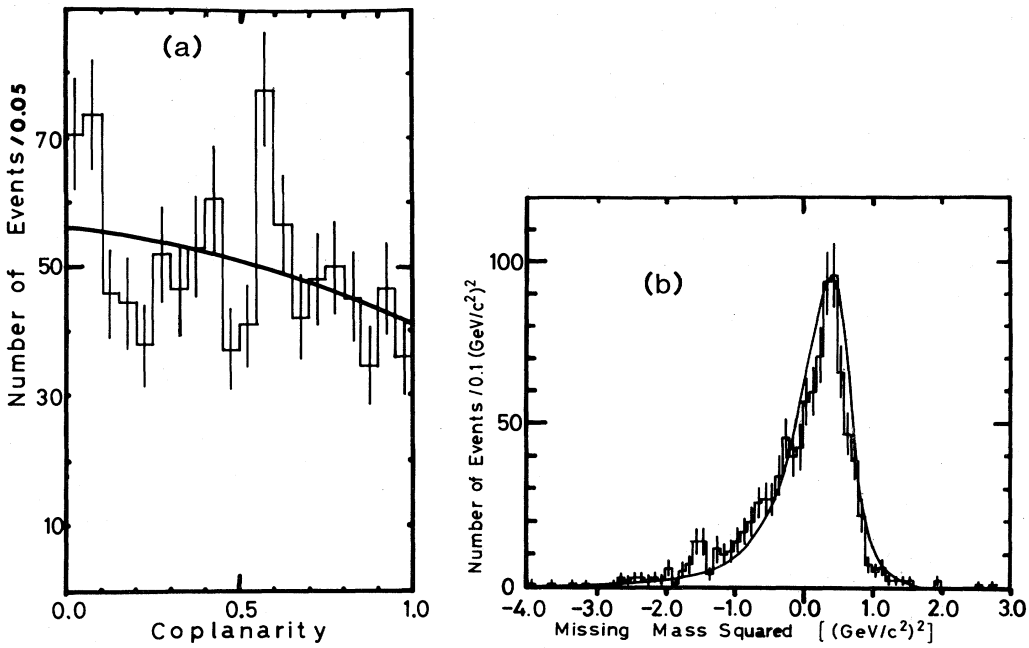


FIG. 1. (a) Coplanarity distribution of three-prong stars and (b) distribution of the missing mass against $\pi^{\pm}\pi^{+}$ assuming that three-prong stars are due to the reaction $\pi^{\pm}p \rightarrow \pi^{\pm}\pi^{+}n$. The solid curves are the result of a Monte Carlo simulation.

We also obtained average branching ratios of $\bar{n}p$ annihilation into $2\pi^{+}\pi^{-}$, $2\pi^{+}\pi^{-}(m\pi^{0}, m \geq 1)$, $3\pi^{+}2\pi^{-}$, and $3\pi^{+}2\pi^{-}(m\pi^{0}, m \geq 1)$ relative to all three- and five-prong star annihilation. They are $(3.2\pm0.5)\%$, $(67.3\pm2.1)\%$, $(5.8\pm0.6)\%$, and $(23.4\pm1.3)\%$. These branching ratios should be compared with the values obtained based on the ratios reported by Caro *et al.*[10] from the charge-symmetric $\bar{p}n$ reactions. They are $(2.9\pm0.3)\%$, $(70.7\pm5.0)\%$, $(7.4\pm2.0)\%$, and $(19.0\pm3.0)\%$. (These values are slightly different from those quoted in Ref. 10, which include one-prong annihilation, and we have adjusted them for the topologies under consideration.) The agreement between the two sets of data is good. From these checks we conclude that the accepted events are not contaminated by the background reactions considered.

There is still a background which is due to a genuine $\bar{n}p$ annihilation reaction by an $\bar{n}$ generated outside the visible region of the bubble chamber, which is accidentally associated with a zero-prong topology. A discussion on the background due to $\bar{n}$ generated in the beam degrader in front of the bubble-chamber beam window will be presented in Sec. V.

## III. KINEMATICAL CONSIDERATION

Because the mass of the $\bar{n}$ and $n$ is slightly larger than that of the $\bar{p}$ and $p$, the kinematics of the reaction is such that there are two c.m. $\bar{n}$ production angles corresponding to a given $\bar{n}$ production angle in the laboratory system. This means that there are two $\bar{n}$ momenta in the laboratory system, one being very much smaller than the other. The actual distribution of the $\bar{n}$ path length was such that almost in all cases the higher momentum would be the correct momentum to choose. This was borne out by the fact that the fitted $\bar{n}$ momentum of all events fitting a four-constraint hypothesis corresponded to the higher momentum solution. Some events fitting a one-constraint hypothesis had the fitted $\bar{n}$ momentum corresponding to the lower momentum solution. Such events were reanalyzed as zero-constraint events using only the direction of the $\bar{n}$, and the momentum of the incident $\bar{p}$ as the known quantities and the higher momentum solution was adopted. The $\bar{n}p$ annihilation stars of these events were put in the category of having more than one $\pi^{0}$. The events which did not fit any hypothesis were analyzed in the same way. The $\bar{n}$ momentum distribution thus obtained is shown in Fig. 2.

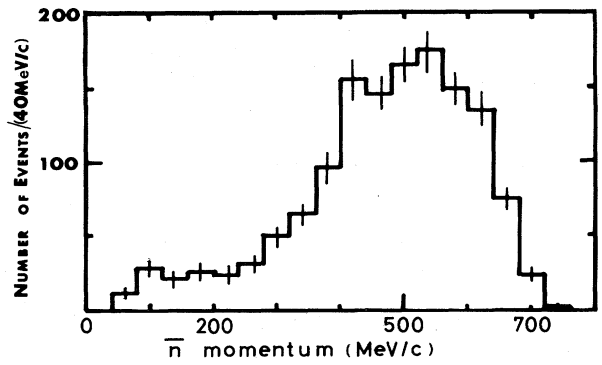


FIG. 2. $\bar{n}$ momentum distribution for all incident momenta.

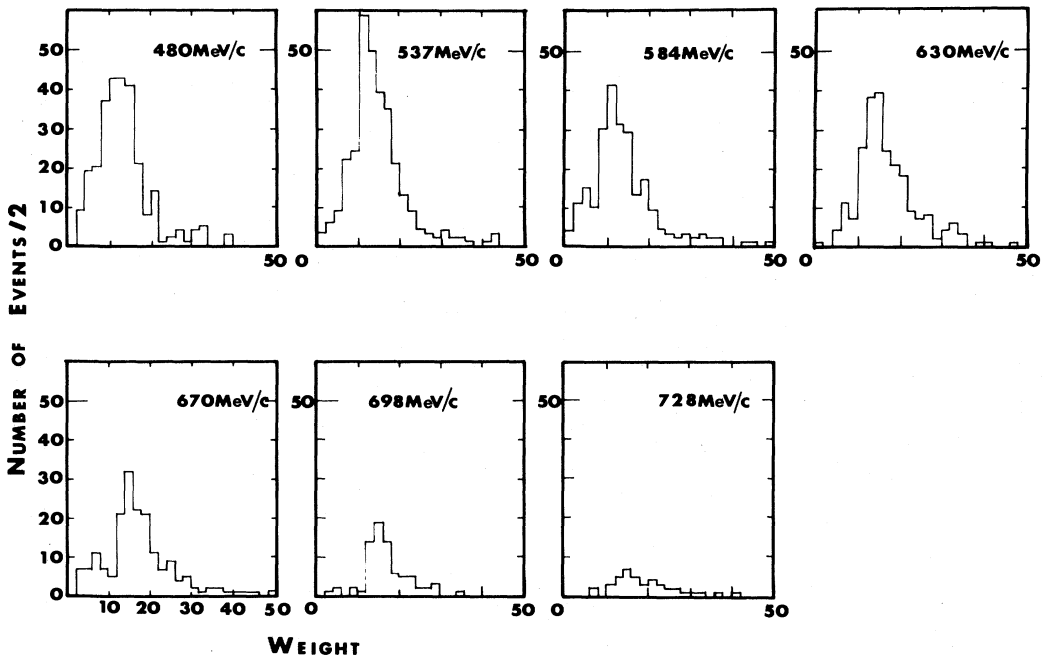


FIG. 3. Weight distributions at all incident momenta. The numbers indicate the incident momenta.

## IV. CROSS SECTIONS

Each observed $\bar{n}p$ annihilation star must be weighted by the inverse of the probability of observing it within the fiducial volume of the bubble chamber.

The probability $P$ that an $\bar{n}$ will produce a three-, five-, or seven-prong star within the potential path $l_p$ between the primary vertex and the boundary of the fiducial volume for $\bar{n}p$ annihilation stars is

$$P=[1-\exp(-l_p N_0 \rho \sigma_{\bar{n}p})]\frac{\sigma_*}{\sigma_{\bar{n}p}} ,$$

where $N_0$ is Avogadro's number, $\rho$ is the density of liquid hydrogen, $\sigma_{\bar{n}p}$ is the total $\bar{n}p$ cross section, and $\sigma_*$ is the cross section for producing a three-, five-, or seven-prong star. The weight $W$ is the reciprocal of $P$, which for our case of $l_p N_0 \rho \sigma_{\bar{n}p} \ll 1$, can be approximated as

$$W \sim \frac{1}{\sigma_* l_p N_0 \rho} .$$

There are two sets of $\sigma_*$ obtained from $\bar{p}d$ interactions,[11,12] which differ by about 15% in normalization from one another. We chose to use the cross sections obtained by Bizzarri *et al.*,[11] which are higher, because they have better statistics and a more detailed account of how they were obtained is given. We fitted the cross sections of Bizzarri *et al.*[11] to the form $\sigma=747\pm9/\sqrt{T}$ ($T$ is $\bar{p}$ kinetic energy), and used the fitted values of the cross section for the weight calculation. Since the two sets do not differ much in their momentum dependence, the choice of $\sigma_*$ should not change the shape of the $\bar{n}$ angular distributions. The distributions of weights are shown in Fig. 3 for all momenta and Fig. 4 shows the total cross section as a function of incident momentum together with the cross sections obtained by Scherer,[5] Hamilton *et al.*,[2] and Bogdanski *et al.*[3] The error bars indicate statistical errors only. In addition there is an uncertainty of about 5% reflecting the uncertainty in the $\sigma_*$ of Bizzarri *et al.*[11] There is also a systematic error of about $+15\%$ due to the choice of $\sigma_*$ as mentioned above. Finally there is a systematic error of at most $-6\%$ due to $\bar{n}$'s generated in the beam degrader, but it is likely to be much smaller than this value as described in Sec. V. Our cross sections are roughly consistent with the much more precise data of Hamilton *et al.*[2]

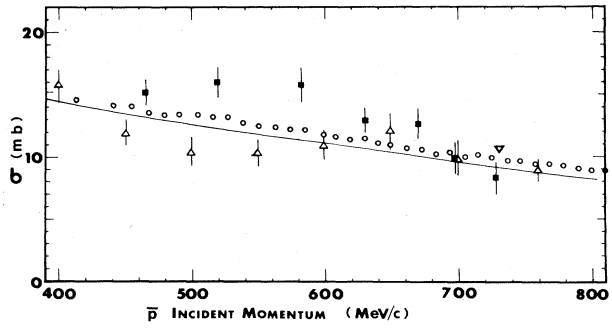


FIG. 4. $\bar{p}p$ charge-exchange cross section vs incident momentum together with other data. Errors are statistical only. ■; this experiment; ○; Hamilton *et al.* (Ref. 2); △; Scherer (Ref. 5); ▽; Bogdanski *et al.* (Ref. 3). The solid curve is the prediction of Bryan and Phillips (Ref. 14) for $L \leq 4$, $J \leq 5$.

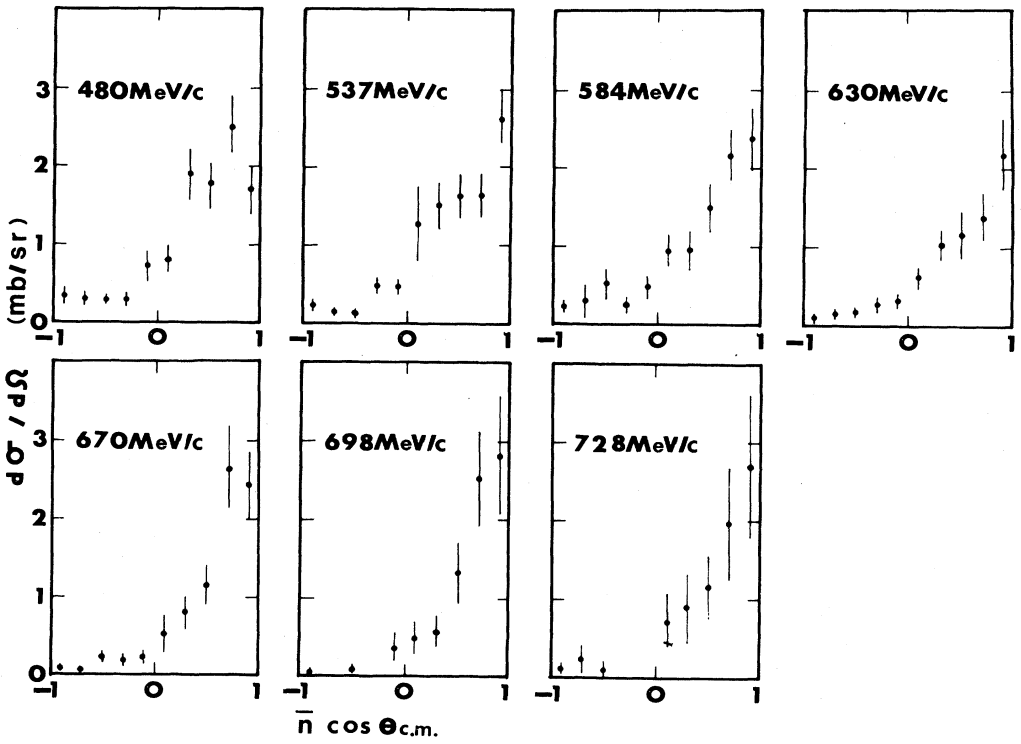


FIG. 5. $\bar{p}p$ charge-exchange differential cross sections normalized to the data of Hamilton *et al.* (Ref. 2).

The $\bar{n}$ c.m. differential cross sections at all momenta normalized to the total-cross-section measurement of Hamilton *et al.*[2] are shown in Fig. 5 and are tabulated in Table I. The errors are statistical only, and there is a systematic error of at most $-6\%$ due to $\bar{n}$'s coming from the beam degrader.

## V. BACKGROUND DUE TO UNASSOCIATED $\bar{n}p$ ANNIHILATION

As mentioned earlier there is a background due to genuine $\bar{n}p$ annihilation stars unassociated with zero-prong vertices. These annihilation stars come mostly from $\bar{n}$ produced in the polyethylene beam degrader placed in front of the bubble chamber. We attempted to estimate this background by assuming that the $\bar{n}$ production by the $\bar{p}$-degrader interaction is proportional to the proton density in the degrader and to the $\bar{p}p$ charge exchange cross section. We then calculated the probability of a zero-prong vertex and an $\bar{n}p$ annihilation occurring in the forward hemisphere of the zero-prong vertex in the same picture. In the calculation the zero-prong cross sections obtained by Sai *et al.*[13] were used. Our estimate shows that even if the probability of an $\bar{n}$ produced in the degrader entering into the bubble chamber is one, the systematic error introduced in the total cross section measurement due to this background is about 6%.

We simulated the distribution of $\bar{n}$'s from the degrader in the fiducial volume by using the actual $\bar{p}$ beam profile and $\bar{n}$ angular distribution of the charge-exchange reac-

TABLE I. $\bar{n}$ differential cross sections for the reaction $\bar{p}p \rightarrow \bar{n}n$ at seven momenta.

| $\cos\theta$ | 480 MeV/$c$ | 537 MeV/$c$ | 584 MeV/$c$ | 630 MeV/$c$ | 670 MeV/$c$ | 698 MeV/$c$ | 728 MeV/$c$ |
|---|---|---|---|---|---|---|---|
| −0.9 | 0.36±0.14 | 0.23±0.06 | 0.24±0.06 | 0.11±0.05 | 0.10±0.04 | 0.06±0.04 | 0.12±0.08 |
| −0.7 | 0.32±0.10 | 0.15±0.05 | 0.32±0.19 | 0.16±0.06 | 0.06±0.03 | 0.00±0.00 | 0.24±0.19 |
| −0.5 | 0.31±0.09 | 0.14±0.06 | 0.51±0.20 | 0.19±0.08 | 0.22±0.09 | 0.09±0.06 | 0.11±0.11 |
| −0.3 | 0.31±0.10 | 0.46±0.13 | 0.31±0.12 | 0.28±0.10 | 0.19±0.09 | 0.00±0.00 | 0.00±0.00 |
| −0.1 | 0.73±0.21 | 0.45±0.11 | 0.46±0.15 | 0.34±0.12 | 0.23±0.09 | 0.37±0.22 | 0.00±0.00 |
| 0.1 | 0.82±0.19 | 1.28±0.45 | 0.93±0.21 | 0.61±0.15 | 0.54±0.23 | 0.48±0.22 | 0.68±0.36 |
| 0.3 | 1.91±0.29 | 1.50±0.27 | 0.94±0.28 | 1.04±0.22 | 0.86±0.21 | 0.59±0.23 | 0.91±0.44 |
| 0.5 | 1.75±0.29 | 1.64±0.26 | 1.52±0.29 | 1.16±0.30 | 1.15±0.25 | 1.33±0.41 | 1.16±0.40 |
| 0.7 | 2.53±0.38 | 1.64±0.25 | 2.19±0.33 | 2.15±0.31 | 2.64±0.51 | 2.53±0.62 | 1.96±0.70 |
| 0.9 | 1.71±0.29 | 2.64±0.35 | 2.38±0.41 | 3.21±0.45 | 2.44±0.41 | 2.83±0.75 | 2.73±0.88 |

tion, and found it to be nearly uniform. Therefore, the $\bar{n}$ produced in the degrader was assumed to be distributed isotropically with respect to unassociated zero-prong vertices. When transformed into the c.m. system an isotropic distribution in the laboratory system remains nearly isotropic with a gradual rise toward the backward direction but dropping rapidly to zero at very backward angles. Thus, if there were a significant background contribution, the $\bar{n}$ differential cross section would show a significant enhancement in the backward direction, which is not the case. We conclude, then, that this background contamination is small, and its effect on the $\bar{n}$ differential cross section, if any, is to uniformly raise it by a very small amount.

## VI. COMPARISON WITH THE BRYAN-PHILLIPS MODEL AND CONCLUSION

Bryan and Phillips proposed a potential model with the $G$-parity-reversed one-boson-exchange (OBE) potential for the nucleon-nucleon interaction and a Woods-Saxon-type imaginary potential to analyze the antinucleon-nucleon interaction.[14] Our earlier analysis of $\bar{p}p$ elastic scattering using the same film as used in this analysis[15] showed that the Bryan-Phillips model was quite successful in reproducing the momentum dependences of the Legendre coefficients for the angular distribution up to $a_4/a_0$. We performed a similar analysis with the $\bar{n}$ angular distributions. We did not need coefficients higher than $a_3$, unlike Scherer,[5] who obtained coefficients up to $a_{10}/a_0$. Figure 6 shows the normalized Legendre coefficents $a_1/a_0$, $a_2/a_0$, and $a_3/a_0$ as functions of incident momentum together with those obtained by Scherer[5] and Bettini *et al.*[7] Our values are also tabulated in Table II. The momentum dependences of our normalized Legendre coefficients fit in well with these other data taken in the neighboring and overlapping momentum regions.

The solid curves in Fig. 5 are the result of the calculation using the Bryan-Phillips model with partial-wave amplitudes up to $L=4$ and $J=5$. The agreement between theory and experiment is only fair, unlike the case of elastic scattering with the same $L$ and $J$.[15] The agreement with $a_3/a_0$ becomes a little better if $L$ is increased to 9. The not-so-satisfactory agreement with theory is probably due to the fact that in the charge-exchange case the difference between the $I=0$ and $I=1$ amplitudes gives the reaction amplitude, while the sum of the two gives the elastic amplitude. Since the large absorptive amplitude is isospin independent, the $I=0$ and $I=1$ amplitudes are nearly equal in magnitude. Therefore, the charge-exchange amplitude is much more susceptible to the choice of the values of the parameters and the assumptions of the model than the elastic scattering amplitude. The poor agreement is probably also due to the fact that the data are not as statistically significant as the elastic-scattering data. The fact that the model agrees well with the total-cross-section measurement of Alston-Garnjost *et al.*[1] and that of Hamilton *et al.*[2] as indicated by the solid curve in Fig. 4, means either the predicted shape of the differential cross section or that of the experimental data is not quite right. The model predicts a dip in the forward direction which cannot be detected experimentally within our limited statistics. Such a dip was observed experimentally,[3,4] but the model did not agree with the observed shape of the angular distributions.

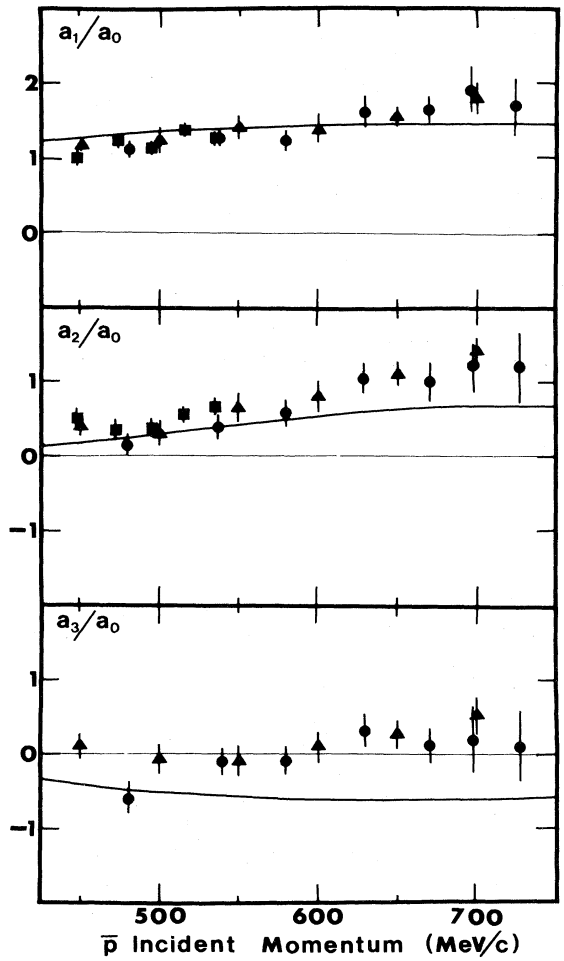


FIG. 6. Legendre coefficients as functions of incident momentum together with other data. ● indicates our data, ▲ the data of Scherer (Ref. 5), and ■ the data of Bettini *et al.* (Ref. 7). The solid curves are the predictions of Bryan and Phillips (Ref. 14) for $L \leq 4$, $J \leq 5$.

There is clearly a need for better experimental data and

TABLE II. Values of the Legendre coefficients $a_1/a_0$, $a_2/a_0$, and $a_3/a_0$ at seven momenta.

| Momentum (MeV/$c$) | $a_1/a_0$ | $a_2/a_0$ | $a_3/a_0$ |
|---|---|---|---|
| 480 | 1.12±0.12 | 0.14±0.15 | −0.61±0.18 |
| 537 | 1.31±0.12 | 0.39±0.18 | −0.12±0.18 |
| 584 | 1.24±0.15 | 0.58±0.17 | −0.10±0.19 |
| 630 | 1.63±0.16 | 1.03±0.20 | 0.30±0.24 |
| 670 | 1.65±0.20 | 0.98±0.23 | 0.10±0.24 |
| 698 | 1.84±0.30 | 1.18±0.37 | 0.17±0.44 |
| 728 | 1.70±0.38 | 1.18±0.46 | 0.10±0.50 |

a theory capable of predicting both elastic and charge-exchange reactions. However, considering the somewhat *ad hoc* nature of the imaginary potential in the Bryan-Phillips model, the partial agreement with the data is almost surprising and renders support for this type of the OBE-plus-absorptive-potential approach to the understanding of the antinucleon-nucleon interaction.

## ACKNOWLEDGMENTS

We are grateful to the operating crews of the Brookhaven Alternating Gradient Synchrotron and the 30 in. bubble chamber for their assistance during the exposure, and to the scanning and measuring crews of the Universities of Massachusetts and Tokyo for their dilligent work. We are also grateful to J. Button-Shafer, R. Carson, S. Hertzbach, and R. Kofler of the University of Massachusetts who participated in the early stage of this experiment, and to R. Phillips for advice. One of us (S.S.) wishes to acknowledge with thanks the financial support from the Japan Society for the Promotion of Science. The computation for this work was performed at the Computer Centers of University of Tokyo and KEK. This work was supported in part under the auspices of the U.S. Department of Energy and the Meson Science Laboratory, University of Tokyo, and by grants from the Toray Science Foundation, the Kurata Foundation, and the Japanese Ministry of Education, Science, and Culture.

---

*Present address: Wilson Laboratory, Cornell University, Ithaca, New York.

[1]M. Alston-Garnjost *et al.*, Phys. Rev. Lett. 35, 1685 (1975).
[2]R. P. Hamilton *et al.*, Phys. Rev. Lett. 44, 1179 (1980).
[3]M. Bogdanski *et al.*, Phys. Lett. 62B, 117 (1976).
[4]H. Kohno *et al.*, Nucl. Phys. B41, 485 (1972).
[5]V. R. Scherer, Ph.D. thesis, University of Wisconsin, 1974.
[6]R. Bizzarri *et al.*, Nuovo Cimento 54A, 456 (1968).
[7]A. Bettini *et al.*, Report No. CERN/EP/PHYS 78-32, 1978 (unpublished).
[8]S. Sakamoto *et al.*, Nucl. Phys. B158, 410 (1979).
[9]R. Bizzarri *et al.*, Nuovo Cimento 20A, 393 (1974).
[10]D. E. Caro *et al.*, Nucl. Phys. B90, 221 (1975).
[11]R. Bizzarri *et al.*, Nuovo Cimento 22A, 225 (1974).
[12]R. D. Burrows *et al.*, Aust. J. Phys. 23, 819 (1970).
[13]S. Sai *et al.*, Nucl. Phys. B213, 371 (1983).
[14]R. A. Bryan and R. J. N. Phillips, Nucl. Phys. B5, 201 (1968); B7, 481(E) (1968).
[15]S. Sakamoto *et al.*, Nucl. Phys. B195, 1 (1982).